The Journal of Chemical Physics ARTICLE pubs.aip.org/aip/jcp

Atomistic simulations of calcium aluminosilicate interfaced with liquid water

Cite as: J. Chem. Phys. 159, 104704 (2023); doi: 10.1063/5.0164817
Submitted: 24 June 2023 • Accepted: 15 August 2023 •
Published Online: 11 September 2023

F. Vuković,[1] N. A. Garcia,[1] S. Perera,[1] M. Turchi,[2,a)] M. P. Andersson,[2] M. Solvang,[3] P. Raiteri,[4,b)] and T. R. Walsh[1,b)]

AFFILIATIONS

[1] Institute for Frontier Materials, Deakin University, Geelong, VIC 3216, Australia
[2] Department of Chemical and Biochemical Engineering, Technical University of Denmark, Kgs. Lyngby 2800, Denmark
[3] Group Research and Development, ROCKWOOL A/S, 2640 Hedehusene, Denmark
[4] Curtin Institute for Computation/The Institute for Geoscience Research (TIGeR), School of Molecular and Life Sciences, Curtin University, Perth, Western Australia 6845, Australia

[a)] **Current address:** Laboratory of Multiscale Studies in Building Physics, Swiss Federal Laboratories for Materials Science and Technology, EMPA, Dübendorf 8600, Switzerland.
[b)] **Authors to whom correspondence should be addressed:** P.Raiteri@curtin.edu.au and tiffany.walsh@deakin.edu.au

ABSTRACT

The dissolution behavior of calcium aluminosilicate based glass fibers, such as stone wool fibers, is an important consideration in mineral wool applications for both the longevity of the mineral wool products in humid environments and limiting the health impacts of released and inhaled fibers from the mineral wool product. Balancing these factors requires a molecular-level understanding of calcium aluminosilicate glass dissolution mechanisms, details that are challenging to resolve with experiment alone. Molecular dynamics simulations are a powerful tool capable of providing complementary atomistic insights regarding dissolution; however, they require force fields capable of describing not-only the calcium aluminosilicate surface structure but also the interactions relevant to dissolution phenomena. Here, a new force field capable of describing amorphous calcium aluminosilicate surfaces interfaced with liquid water is developed by fitting parameters to experimental and first principles simulation data of the relevant oxide-water interfaces, including *ab initio* molecular dynamics simulations performed for this work for the wüstite and periclase interfaces. Simulations of a calcium aluminosilicate surface interfaced with liquid water were used to test this new force field, suggesting moderate ingress of water into the porous glass interface. This design of the force field opens a new avenue for the further study of calcium and network-modifier dissolution phenomena in calcium aluminosilicate glasses and stone wool fibers at liquid water interfaces.

I. INTRODUCTION

Calcium aluminosilicate (CAS: $CaO–Al_2O_3–SiO_2$) glasses are a family of materials comprising an amorphous network of aluminum, silicon, and oxygen, in which calcium acts as a network modifier. Of particular interest is stone wool fiber, an amorphous CAS-based material that is used for many applications such as products for thermal and acoustic insulation of buildings, facade claddings, fire protection, and, in addition, growing substrates in the horticultural industry and urban water management solutions. Understanding and controlling the dissolution behavior of such stone wool fibers in humid environments is a critical aspect in applications for both ensuring product stability under humid conditions and limiting the health impacts of released respirable fibers during handling of the product in various workplaces (i.e., production, installation, and demolition). Despite experimental interrogation,[1] a complete understanding of dissolution for the more complex stone wool fiber composition has yet to be achieved, due in part to current limitations in simulation approaches. Determination of the atomic-scale surface structural features of CAS glass fibers is, therefore, a key step in predicting the dissolution behaviors of these materials. However, this task is not readily addressed using experimental efforts alone, and atomic-scale molecular dynamics (MD) simulations can provide powerful and complementary insights into the characteristic interfacial structural features of glasses relevant to dissolution phenomena.[2,3]

The dissolution free energies of network modifiers from the glass interface are a critical aspect of the complete dissolution behavior of CAS glasses,[1] and can be explored using classical MD simulations with free energy perturbation methods.[4,5] The veracity of the outcomes produced by MD simulations rests in part on the mathematical expressions and their corresponding parameter sets, referred to collectively as a force-field (FF) to model interparticle interactions. FFs exist on a spectrum of system suitability and capability, where one typically must trade the complexity of the description with computational cost. Reactive FFs, i.e., FF capable of forming and breaking covalent bonds, based on the ReaxFF framework,[6] have been developed for several elemental subsets of the CAS composition, e.g., Ca/Al/H/O/S for hexacalcium aluminate trisulfate hydrate,[7] Si/O for silicon oxides,[8] Ca/O/H for calcium oxides,[9] among others.[10–12] Although a combination of some of these parameter sets has previously been used to study structural details of calcium aluminosilicate hydrates,[13] this approach lacks robust parameter benchmarking in addition to being computationally expensive and, therefore, is not viable for simulation of many-thousand atom CAS glass–liquid water systems on the timescale of tens of nanoseconds.

Non-reactive FFs that employ simpler two- and three-body particle interactions are a computationally efficient alternative for both modeling bulk glasses and the glass–water interface. In principle, it is possible to combine a FF for liquid water and several FFs that are able to describe CAS glasses, although in practice, the intended task of calculating the dissolution free energy of the network modifier Ca^{2+} ions from the surface can impose restrictions on how this can be achieved. For example, CLAYFF[14] would, in principle, provide a description of CAS glass; however, CLAYFF supports several different partial charge values for Ca^{2+} that depend on its surrounding environment. In practical terms, this is problematic for calculating the free energy of dissolution because the required transit of the ion from the solid to the liquid cannot involve a change in the partial charge of the dissolved ion.

The Guillot–Sator (GS) FF[15] is a non-reactive and non-polarizable FF developed specifically to model basaltic melts (not solid glass) relevant to CAS and stone wool compositions, and has previously been used by Turchi *et al.*[16] to study various CAS glass compositions related to stone wool fibers. The GS FF has the added advantage of parametrization that provides for the simulation of stone wool fiber composition, notably featuring parameters allowing the incorporation of Mg^{2+}, Fe^{2+}, Fe^{3+}, Na^{+}, and K^{+} into CAS-like compositions, where other similar FFs currently lack this provision.[17,18] Turchi *et al.* reported that the GS FF provides an adequate structural description of bulk CAS glass, predicting, e.g., defect concentrations, proportion of linkage types, and ring size distributions in agreement with experiment. Although the GS FF partial charge description does not permit the calculation of absolute dissolution free energies, *relative* dissolution free energies of the various CAS ion complexes can provide insights regarding the relative free energies of dissolution between differing ion environments in the glass. However, the GS FF does not currently support any description of water, which is needed for the purposes of describing the aqueous CAS glass (or stone wool fiber) interface and is essential for using simulation to predict the dissolution traits of these materials.

Several FFs have been developed to study the aspects of the amorphous silica (SiO_2) under humid conditions. Early MD simulations of glassy silica-water systems reported by Feuston and Garofalini[19] explored the effect of atmospheric water vapor on the silica surface chemistry using a specially developed silica + hydrogen FF[20] in conjunction with the central force water model.[21] The authors interfaced silica surfaces freshly cleaved from the bulk with water at low concentration, finding that defects such as non-bridging oxygen (NBO), two- and three-member rings, and undercoordinated silicon, were more prominent in water-exposed surfaces compared to those prepared in vacuum. Cruz-Chu *et al.*[22] reported simulations of water permeation through amorphous silica nanopores using a FF where water data were fit to experimental water contact angles on amorphous silica surfaces and denoted the "CHARMM water contact angle (CWCA) FF." Mahadevan and Garofalini[23] developed a dissociative water model[24] to use in conjunction with an amorphous silica FF[25] to study the chemisorption of water on the silica surface at low water concentrations. Hassanali and Singer[26] reported MD simulations of an amorphous silica interface with liquid water by incorporating the SPC/E water[27] model into the van Beest, Kramer, and van Santen[28] silica FF. A biomolecular-compatible FF for silica-water interactions was developed by Butenuth *et al.*,[29] suitable for both charge-neutral and deprotonated amorphous silica surfaces. Leroch and Wendland[30] compared the results of several FFs, including ReaxFF, using MD simulation to quantify the adhesion of hydroxylated amorphous silica plates in the presence of liquid water. Others have also used these FFs to study wet silica[31–33] and silica-based glasses.[12,34,35] Among these MD simulation efforts, density-functional tight binding theory, first principles quantum chemistry calculations, and *ab initio* MD simulations have also been used to elucidate water chemistry at silica surfaces.[36–40]

More recently, a force matching algorithm has been used to parameterize a more computationally efficient FF for both dry and hydrated CAS with up to 30 mol. % water content.[41] The authors reported that their FF was able to adequately capture local Ca^{2+} environments and dynamics in both the dry and wet CAS, as well as in liquid water, while reasonable Al behavior proved more challenging to capture due to limitations in the functional forms of the FF. This new FF seems promising, although the authors did not report on the structure or dynamics of liquid water, factors that are significant in the modeling of CAS surfaces interfaced with liquid.

Here, a new FF has been developed to study the dissolution behavior of amorphous CAS glass surfaces immersed in liquid water, denoted herein as "wet-GS." Building on the GS FF[15] that can be used to describe interactions of the CAS, the wet-GS FF extends this by incorporating the SPC/E model[27] for liquid water. A combination of experimental and first-principles quantum chemical data for several oxide-water interfaces was used to parameterize the wet-GS FF. Data for the aqueous interfaces of quartz, corundum, lime, wüstite, and periclase were used to fit water-CAS and water-stone wool interactions. In the cases of quartz and corundum, literature data were available for the purposes of parameter fitting. However, for the wüstite- and periclase-water interfaces, no such data were available in the literature. In these two instances, *ab initio* MD (AIMD)[42,43] simulations were performed in this work to predict interfacial solvent structuring at the oxide-water interface, and subsequently, these data were also used in the fitting process. Once obtained, the new

wet-GS FF was applied in MD simulations of a typical CAS glass-water interface, revealing atomic-scale details of the incipient stages of moisture exposure. The wet-GS FF allows for future study of relative network modifier dissolution free energies present in CAS-based glass fibers, as well as dissolution of the glass network itself.

II. METHODS

A. General simulation details

All MD simulations were performed using the Large-scale Atomic/Molecular Massively Parallel Simulator (LAMMPS) software package,[44] with an integration timestep of 1 fs. Non-bonded interactions were truncated and shifted at a distance of 10 Å, unless otherwise stated, and electrostatic contributions were calculated using the particle–particle particle-mesh method.[45] Simulations performed using the NPT (constant particle, pressure, the temperature) ensemble employed the anisotropic Nosé–Hoover thermostat–barostat[46] to control system temperature and pressure, with $\tau = 0.1$ ps and a pressure damping parameter of 1 ps. Similarly, simulations using the NVT (constant particle, volume, and temperature) ensemble employed only the Nosé–Hoover thermostat using the same τ value. The OVITO software package[47] was used to visualize the trajectories.

AIMD simulations of the wüstite- and periclase-water interfaces were performed using the CP2K software package.[48] These calculations employed full periodic boundary conditions, with electron correlation and exchange treated using the Perdew–Burke–Ernzerhof[49] variant of the generalized gradient approximation. Specific details of these simulations are provided in the supplementary material. Electronic structure calculations of iron oxides are particularly challenging to describe with conventional density functional theory (DFT) approaches due to the highly correlated nature of the iron *d* orbital electrons[50] in such materials. Here, the DFT+U correction method[51] with an effective $U = 3.7$ eV was used for iron, which has previously been used to study iron oxide and related metal-oxide systems.[51–53] Fully periodic cells of these interfaces were modeled using the NVT ensemble, thermostated to 330 K via the Canonical sampling through velocity rescaling algorithm,[54] to overcome the overstructuring of water at 300 K inherent to AIMD methods.[55] Dynamics were run for a total of 12 and 17.5 ps for periclase and wüstite, respectively. Density profiles were calculated by sampling frames every five timesteps, for a total of 4830 and 700 frames for periclase and wüstite, respectively.

B. Parametrization of the wet-GS FF

Simulation of the CAS-water interface requires a FF capable of simultaneously describing interactions inherent to the surface-terminated CAS glass slab, liquid water, and the interaction between the two. To preserve the CAS glass network (which was produced using the GS FF), the SPC/E water model was combined with the original GS FF by fitting the CAS-water cross-terms to data sourced for several oxide-water interfaces. Hydroxyl terms were also required in the wet-GS FF since it is physically reasonable to expect the presence of surface hydroxyls on a cleaved CAS glass surface exposed to water. The combination of the GS, SPC/E, and Morse potentials was chosen because of the specific requirements of each of the components of the interfacial system, namely the glass, liquid, and surface hydroxyls, respectively. To elaborate, the Buckingham potential is used for the glass material because use of a Lennard-Jones potential for the glass would lead to serious and incorrect structural reorganization of the glass network, and the GS potential is based on the Buckingham form. The SPC/E water potential is described by the Lennard-Jones potential and is again fine-tuned for performance in describing liquid water. Finally, the Morse potential was found to be essential for satisfactory description of the surface hydroxyls and follows a similar philosophy used in the development of the CLAYFF force-field. All FF parameters are reported in the supplementary material.

Five oxide-water interfaces were modeled to parameterize the calcium, aluminum, silicon, iron, magnesium, and oxygen GS-water cross terms: lime, quartz, corundum, wüstite, and periclase, respectively. For these systems, non-bonded interactions were truncated and shifted at a distance of 10 Å. Although iron and magnesium are not present in the CAS composition studied in the current work, both can be found in related stone wool fiber materials, which are targets for future investigations. FF parameters were fitted by comparing interfacial water structuring data at the oxide-water interface against various experimental and DFT data reported in the literature.

In the case of wüstite and periclase, AIMD simulations of oxide-water interfaces were performed because no data related to these aqueous interfaces are currently available in the literature. It is reiterated here that the GS FF was not designed to model solid crystalline systems (it was designed to model melts); therefore, these crystalline oxide-water interface simulations were performed only as a means to fit the glass-water cross terms.

Parameters to describe the interactions between surface hydroxyls, water, and the GS FF were fit using vertical density profiles at the crystalline oxide-water interface (i.e., along the direction normal to the surface plane). Initial parameters were based on those published by Armstrong *et al.*[56] Since the forms of the potentials used in this work are similar, this resulted in minor adjustments of the parameters, which were fitted manually. The initial structures of the oxide-water interfaces were prepared by packing water molecules in a spatially randomized fashion into the vacuum gap along the *z* dimension of the unit cell (perpendicular to the oxide surface plane). MD simulations for lime, quartz, and corundum were performed in the NPT ensemble at 300 K and 1 atm of pressure. The wüstite and periclase surfaces were not structurally stable using the GS FF (consistent with the fact that GS is not designed to model crystalline materials), and as such, the oxide atoms were restrained to their crystal lattice sites using harmonic functions with a force constant of 1 eV/Å^2 to stabilize the crystal structure. These simulations were carried out in the NVT ensemble at 300 K, with the *z* dimension of the simulation cell adjusted to recover the appropriate liquid water density in the bulk water region of 0.0334 Å^{-3}. The oxide-water interfaces were then subjected to 1 ns of dynamics. Full simulation details for each system can be found in the supplementary material.

Density profiles were calculated using frames collected every 1 ps over the final 950 ps of dynamics sampling for a total of 950 frames, thereby allowing the cell dimensions to equilibrate prior to the calculation. An approximate bin width of 0.1 Å was used, noting that the specific bin width varied slightly as the cell dimensions fluctuated during NPT simulation. Silanol and aluminol angle

distribution data for the quartz- and corundum-water interfaces, respectively, were also calculated using the same trajectory interval and sampling rate.

C. Calcium aluminosilicate-water interface simulations

A sample of bulk CAS glass was prepared as per the methodology of Turchi *et al.*,[16] and the composition used herein corresponds to "CAS1," i.e., 43.5 mol. % CaO, 13 mol. % Al_2O_3, and 43.5 mol. % SiO_2. A brief summary of the CAS glass slab creation process is provided herein. The compositions of both the bulk and resultant CAS glass slabs after surface termination are presented in Table I. The first stage in preparing the CAS glass slabs is the surface creation and annealing from the bulk. Details of the process for creating the bulk material have been reported by Turchi *et al.*,[16] and a full description of the surface creation protocol, including sensitivity analysis of the surface creation parameters, will be provided in a future report. Note that the CAS glass slab structure used for the current study was created solely for the purposes of testing the CAS-water interfacial structure. A more in-depth study regarding CAS glass surface creation computational protocols is currently in preparation.

The bulk CAS glass model comprised ~5000 atoms in a fully periodic orthorhombic cell of approximate dimensions $50 \times 50 \times 50$ Å^3. A slab ~25 Å thick was cut from this bulk glass sample, and a vacuum gap was introduced along the z unit cell dimension, creating two unique CAS surfaces normal to the z direction. Atoms located in the central bulk region of this slab were then frozen while the free surfaces (defined by the top ~9 Å of the slab exterior) were annealed at 1500 K prior to being cooled to 300 K at a rate of 2.25 K ps^{-1}. The CAS glass slabs in this state will be herein referred to as non-treated slabs. These non-treated slabs were stable under anisotropic NPT MD simulation dynamics with the vacuum gap maintained in place.

The non-treated slabs were then subjected to a surface termination procedure to more realistically capture the structure of the CAS glass surface upon exposure to ambient humidity. This procedure was a three step process in which (i) atoms that define the surface atomic sites on the CAS surfaces were identified, (ii) all non-bridging oxygen (NBO) atoms at the surface sites were protonated, and (iii) all surface-exposed two- and three-member rings were opened by removing one ring oxygen and hydroxylating the ring atoms that were coordinated with the deleted oxygen. To define the CAS surface, a spatial grid normal to the z was established with a bin width of 5 Å in both the x and y dimensions. The bounding z coordinates of the slab were then calculated for each bin, using the lowest and highest CAS atom positions to define the bottom and top surfaces, respectively.

TABLE I. Composition percentages and total number of atoms of the bulk, and surface treated CAS glass slab.

	Ca	Al	Si	O	H	No. of atoms
Non-treated slab	15.4	9.2	15.4	60.0	0.0	5585
Treated slab	12.5	8.9	14.9	58.3	5.4	5783

Using the above-mentioned definition of the top and bottom CAS glass slab surfaces, all NBO within a depth of 2 Å of the surfaces were protonated. Hydrogen atoms were assigned a charge of 0.4725 e, which is half the magnitude of the oxygen charge as per the original GS FF. A key consideration was the maintenance of the charge neutrality of the system, and to this end, only an even number of NBOs were protonated, N_{NBO} ensuring that charge neutrality could be maintained by $N_{NBO}/2$ Ca atoms (since the charges of the calcium and oxygen atoms in the GS FF are related). The Ca atoms flagged for removal were randomly selected so as to not introduce spatial charge concentrations by favoring Ca removal in either the bulk or at the surface. At this stage of the procedure, the CAS slab also contained 15 free oxygen atoms, which were removed in addition to a further 15 randomly selected Ca atoms (again for charge neutrality maintenance). In total, 246 surface NBOs were protonated, and a total of 138 Ca atoms were removed from the slab during the surface termination procedure (Table I).

In the final stage of the procedure, two- and three-member rings at the surface were opened and hydroxylated. Surface rings were defined to be a ring with any ring-member atom within a surface depth of 2 Å of either the top or bottom surfaces. The selection of the oxygen to be removed was determined by a pair of hierarchical conditions: (i) the lowest coordinated oxygen, and (ii) the oxygen closest to the defined surface level. For example, considering a ring comprising two oxygen atoms, for the choice between one ring oxygen atom having a lower coordination number and a location further away from the surface vs another with a higher coordination number closer to the surface, the former would be selected. These criteria were devised with the intent to open the ring at the weakest part of the network structure, as it is expected that under ambient air conditions, the least-bound oxygen would be the likely location of the ring opening event. Since the ring is opened via oxygen removal, the two connecting ring atoms are then hydroxylated, resulting in a net zero change in total system charge. A total of three two-member and thirty three-member rings were opened on both slab surfaces. The surface treatment process resulted in an approximate hydroxyl surface density of 7 nm^{-1}.

As 138 Ca atoms were removed from the surface-terminated slab, the system needed to be carefully relaxed to an equilibrium state in vacuum prior to interfacing with liquid water. Installed hydroxyls (including the protonated NBO) were restrained at their positions with temporary harmonic bonds, with force constants and bond lengths tuned to recover the approximate GS interactions between O–Al and O–Si (as provided in the supplementary material). First, an energy minimization was performed, followed by 400 ps of *NPT* dynamics at 300 K with an anisotropic barostat set at 1 atm pressure in the x and y dimensions while maintaining the vacuum gap by keeping the z dimension fixed. This process allowed the Ca to reconfigure and settle after the Ca deletion step arising from the surface termination process. Next, the harmonic hydroxyl bonds were removed returning all interactions between hydroxyl oxygen and the CAS network to the original GS description. The system was then subjected to a further 200 ps of *NPT* dynamics using the same thermostat and barostat conditions. During this final stage of *in vacuo* simulation, all hydroxyl oxygens remained connected to their original attachment sites. A small degree of network rearrangement during this surface relaxation protocol was observed, which was quantified via coordination, linkage, and density profile analysis.

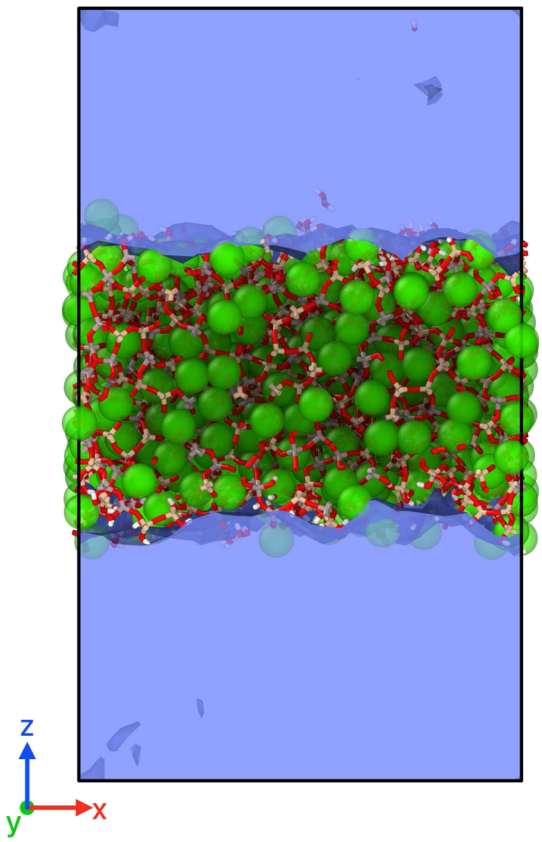

FIG. 1. Surface terminated CAS glass slab interfaced with water after 500 ps of *NPT* simulation, where water is represented as a blue volume, calcium with green spheres, and network silicon, aluminum, and oxygen are represented as a bond network in beige, gray, and red, respectively. Black solid lines indicate the boundary of the periodic cell.

This final state of the CAS glass slab is herein referred to as the "treated slab." Finally, the treated CAS slab was interfaced with liquid water by increasing the vacuum gap ~74 Å, which was subsequently packed with 4932 water molecules using the Packmol software package,[57] at approximately the appropriate density of water at room temperature and ambient pressure (0.0334 molecules $Å^{-3}$). Figure 1 shows an image of the CAS-water interface following this process.

Initial *NPT* simulations of the CAS-water interface exhibited a temperature differential between the CAS slab and the liquid water, a simulation artifact commonly known as the "cold solute, hot solvent" problem.[58] A chain of five Nosé–Hoover thermostats thermostats was not able to resolve the temperature differential. Instead, dual Nosé–Hoover thermostats were employed to correct the issue, one acting on the CAS slab and another on the liquid water.[59] The center of mass linear momentum of the CAS glass slab was removed every 10 ps to prevent translational drift of the slab within the unit cell.

Trajectory analyses of the CAS-water interface MD simulations were performed using a combination of the MDAnalysis python package[60–62] and in-house codes. Hydrogen bonding data were calculated for hydrogen bonds between CAS and water only, using a donor–acceptor distance cutoff of 3 Å and a donor-hydrogen-acceptor angle cutoff of 150°. Hydrogen bonds were calculated at every ps of simulation time, and data were smoothed using a Savitzky–Golay (SG) filter[63] with a sampling window of 601 and a polynomial order of 3. The lifetimes of each individual hydrogen bond were calculated using an intermittency of 2 ps, i.e., if a particular hydrogen bond was broken for one frame and then re-established in the next, this would be considered a continuous hydrogen bond.

Accurate calculation of water absorption at the nanoscale is challenging for any amorphous solid with intrinsic surface roughness. Here, a proxy measure of the CAS surface is used to provide an estimate of the number of water molecules absorbed during MD simulation. The height or z-coordinate of each surface of the CAS glass slab is defined to be located at the hydroxyl oxygen number density peak (which was smoothed for the peak detection algorithm using the SG filter with sampling window = 201 and polynomial order = 3), since these groups are exclusively located at the CAS surface. Water with a z-coordinate between the two defined CAS surface planes was then considered to be absorbed.

III. RESULTS AND DISCUSSION

A. Oxide-water interfaces and wet-GS force field creation

The GS FF was modified to accommodate the SPC/E water model to facilitate the simulation of amorphous CAS glasses in the presence of liquid water. This new FF is referred to as the wet-GS FF. Data from five oxide-water interfaces were used to parameterize cross-terms between water and the GS description of calcium, silicon, aluminum, oxygen, magnesium, and iron. For all five oxides, the crystal interfaces were created based on experimental crystal structures and cleaved at the (001) plane, except quartz, which was cleaved at the (101) plane. Dangling oxygen atoms at the corundum and quartz terminating surfaces were passivated to create surface hydroxyls. MD simulations of these oxide slabs interfaced with bulk liquid water were performed to obtain interfacial solvent structuring data at the oxide-water interface, which was then used to fit the wet-GS FF parameters to DFT and experimental water structure data. In the case of wüstite and periclase, no interfacial water structure data were available; hence, AIMD simulations of these oxide-water interfaces (of reduced unit cell size relative to the MD simulations) were performed in this work to provide the data required for fitting.

Figure 2 shows density profiles of all atom types present in each interface, calculated via MD simulation with the wet-GS FF (solid lines) and AIMD simulation (dashed lines). All density profiles have been plotted using the last crystal lattice oxygen peak as a baseline, except for quartz, which uses the third-last silicon peak as a baseline value to facilitate comparison with literature data. The values of the first water peak locations are presented in Table II.

The wet-GS FF produced a first peak in the vertical density profile of the lime-water interface at a distance distance of 2.71 Å from the surface crystal lattice oxygen layer, slightly greater than the value reported by de Leeuw *et al.*,[64] who used DFT to calculate the adsorption energy and water structure of water on the (001) lime surface. However, these DFT calculations were performed for a water monolayer, not bulk liquid water. Furthermore, the authors reported that

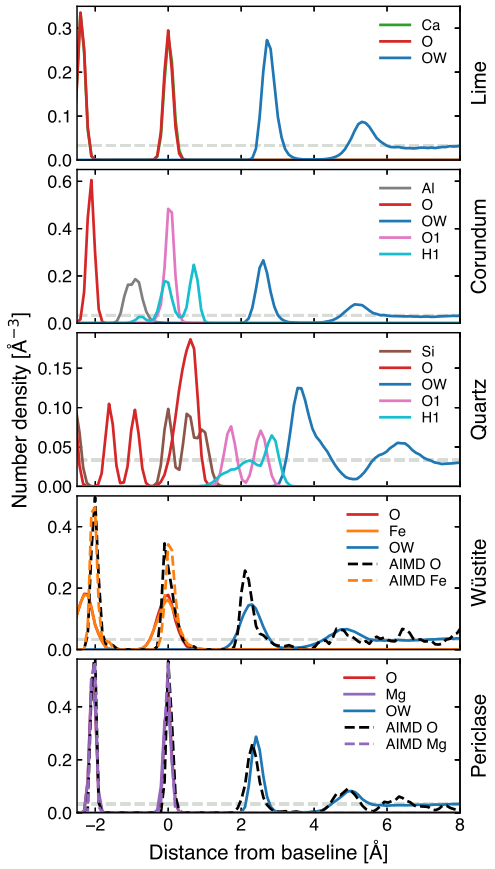

FIG. 2. Number density profiles of all five oxide-water interfaces calculated via MD simulations using the wet-GS FF are shown with solid colored lines, where each color is specific to a particular element. Note that "OW" refers to water oxygen and that "O1" and "H1" refer to oxygen and hydrogen atoms belonging to hydroxyl groups, respectively. The dashed gray horizontal line indicates the experimental bulk water density at 300 K. To facilitate comparison with experimental and first principles literature data, density profiles are plotted relative to a baseline peak, which is the last crystal lattice oxygen peak in all materials, except for corundum and quartz, which are set to the surface hydroxyl peak and the third-last silicon peak, respectively. Density profiles calculated from AIMD simulations are shown with dashed lines.

hydroxylation did not occur in their simulations, whereas lime is known to be unstable and dissolves readily in liquid water.[65–67]

For corundum, the first water peak was located 2.61 Å from the surface hydroxyl oxygen surface for wet-GS. Ridley and Tunega[68] reported AIMD simulations of liquid water interfaced with the (001) corundum surface, indicating an average distance of 2.63 Å between the surface hydroxyl oxygens and the first water peak at the interface, in good agreement with the wet-GS value. Experimental x-ray reflectivity measurements reported by Catalano[69] suggest a slightly closer first water peak at 2.5 Å, while DFT calculations of two-layer water at the corundum interface performed by Janeček *et al.*[70] report a further first water peak at 2.72 Å.

TABLE II. First water density peak locations relative to the baseline as shown in Fig. 2, where † denotes values calculated in this work; all values are in Å. All crystal surfaces are in the (001) orientation, except for Quartz, which is (101). References for the literature values are as follows: [a]Ridley and Tunega,[68] [b]de Leeuw *et al.*,[64] [c]Janeček *et al.*,[70] [d]Bellucci *et al.*,[71] [e]Jug, Heidberg, and Bredow,[73] [f]Catalano,[69] [g]Bellucci *et al.*[71]

	Lime	Corundum	Quartz	Wüstite	Periclase
MD†	2.71	2.61	3.55	2.31	2.41
AIMD†	···	···	···	2.14	2.33
AIMD	···	2.63[a]	···	···	···
DFT	2.62[b]	2.72[c]	3.65[d]	···	2.24 ± 0.1[e]
Expt.	···	2.5[f]	3.4 ± 0.01[g]	···	···

MD simulations with wet-GS of the water-quartz (101) interface yield a distance of 3.55 Å between the third-last crystal aluminum layer and the first water layer. DFT simulations and experimental XR data reported by Bellucci *et al.*[71] bound the wet-GS value with water peaks located at 3.65 and 3.40 (10) Å, respectively.

Wet-GS FF parameters were also fitted for iron and magnesium. Although these elements are not present in the CAS composition studied in this work, they can be found in stone wool fibers, which are compositionally close to the CAS samples considered here. Figure 2 shows both number density profiles calculated from both the wet-GS MD simulation data in solid lines and the AIMD simulations in dashed lines. Wet-GS values for both wüstite and periclase first water layer locations at 2.31 and 2.41 Å, respectively, were slightly greater than the AIMD values at 2.14 and 2.33 Å. Given that both iron and magnesium generally form very small fractions relative to silicon, aluminum, oxygen, or calcium in amorphous glasses that are most closely related to CAS, the currently fitted parameters for iron and magnesium are considered sufficient as further manipulation would detrimentally impact the other oxide-water interfaces. A description of all the terms and parameter values of the wet-GS FF can be found in the supplementary material.

This FF has been fitted to recover the interfacial solvent structuring at a series of relevant oxide interfaces. Therefore, it is not reasonable to expect good performance from the current FF outside the remit of describing structural features, which is typical of many FFs. Other FFs have different specialties, for example, to reproduce the binding energy and site preference of adsorbates.[72]

B. CAS-water interface

The CAS slab was constructed by cleaving a fully periodic bulk CAS model in the (001) plane to create two free surfaces. These surfaces were then subjected to the ring-opening and hydroxylation protocols outlined in the Methods. Figure 3 shows the change in coordination between the pre-surface treated CAS (blue) and the post-surface treated CAS slab (orange) for aluminum, silicon, and oxygen present in the CAS, shown in panels (a)–(c), respectively. In general, only slight changes in network aluminum and silicon can be observed. Turchi *et al.*[16] provide a comprehensive study of the bulk properties of the CAS used here, which maps to the "CAS1" composition in their work. Figure 3(c) shows that a significant fraction of NBO (or singly coordinated oxygen) has been converted to two- and three-fold coordinated oxygen, which is the result of the

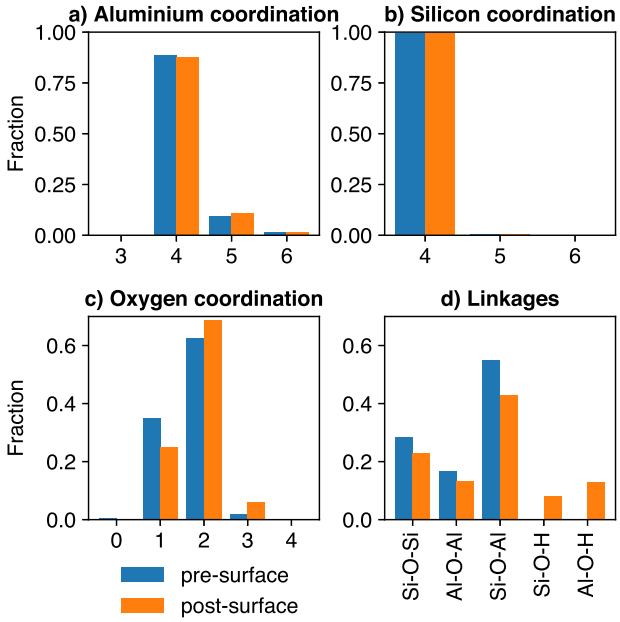

FIG. 3. Panels (a)–(c) show coordination number fractions of aluminum, silicon, and oxygen, respectively, for the pre-surface (blue) and post-surface treated CAS slab (orange). Fractions of linkages present in CAS shown in panel (d).

surface-termination protocol where all NBOs within 2 Å of the free surfaces were protonated.

Linkages present in the network were also quantified pre- and post-surface treatment, as shown in Fig. 3(d). Approximately equal fractions of Si–O–Si and Al–O–Al linkages were opened and converted to terminal hydroxyl groups, whereas a greater fraction of Al–O–Si groups was opened for hydroxylation. It is noted that linkages may have also changed during the equilibration of the surface termination process, in addition to the ring opening. A greater number of Al–O–H groups were present after surface-termination compared to Si–O–H groups, where ~65% of all hydroxyls installed form Al–O–H groups. The proportion of Al–O–Al linkages indicates violation of the Al avoidance principle; however, these data are consistent with both experimental estimates[74–77] and previous simulations[16] of bulk CAS material. The surface-terminated CAS slab was then interfaced with liquid water at near 300 K, 1 atm water density, resulting in a 3D periodic unit cell, which is shown in Fig. 1 of Sec. II. The MD simulation of the CAS-water interface was run for a total of 25 ns in the anisotropic *NPT* ensemble at a temperature of 300 K and a pressure of 1 atm to model the incipient stages of contact between CAS and bulk liquid water. Unit cell dimensions were found to stabilize after ~300 ps of dynamics. A few small fragments, such as the hydroxyl groups of the CAS slab, were found to dissolve almost immediately and remained detached from the main CAS network throughout the simulation. However, the vast majority of the surface hydroxylation and CAS network structure remained intact throughout the entire 25 ns of MD simulation.

Figures 4(a) and 4(b) show number density profiles for separate atom types calculated at 1 and 24.5 ns of simulation, respectively. Intrinsic roughness is present on both the upper and lower CAS surfaces of the slab. Using the network oxygen number density profile (red) as an approximate measure of CAS interphase depth, the lower surface is about 15 Å thick, with the upper interphase estimated to be around 10 Å. Overall, no significant CAS network change can be observed in the density profiles, suggesting that the CAS surface remains stable in contact with liquid water throughout the simulation. Water density is concentrated at the CAS surfaces; however, the intrinsic roughness makes calculation of the water layer distance from the CAS surface via 1D density profiles challenging. The water

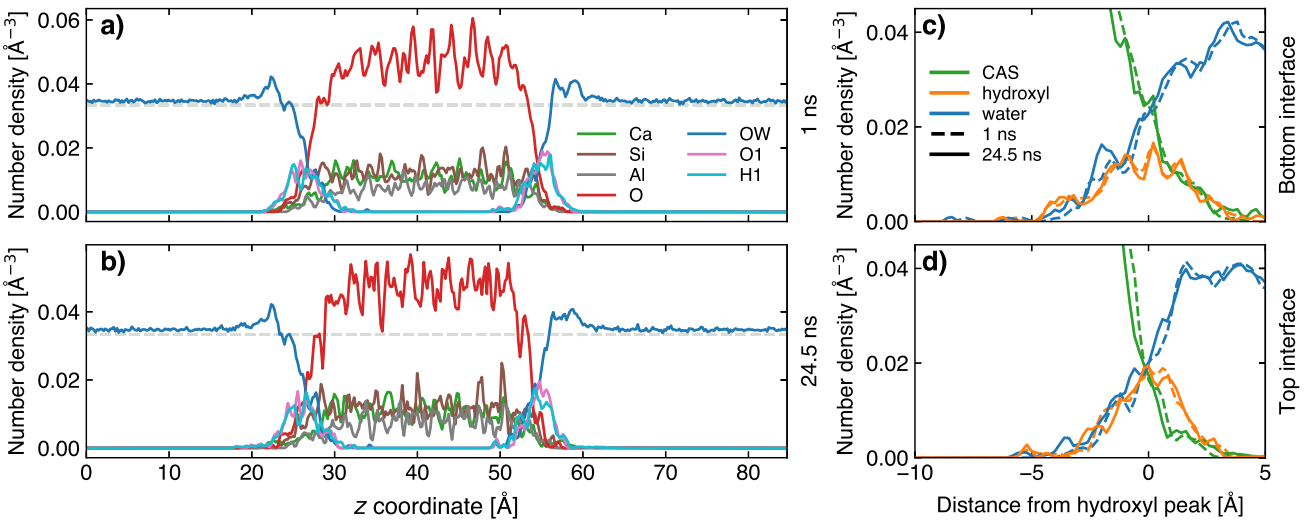

FIG. 4. Number density profiles of each atom type in the CAS-water interface after 1 ns [panel (a)], and 24.5 ns [panel (b)] of dynamics. Number density profiles of the two unique CAS-water interfaces shown in panels (c) and (d) where 1 ns profiles are indicated by dashed lines and 24.5 ns profiles by solid lines. For panels (c) and (d), the CAS profile includes network oxygen, calcium, aluminum, and silicon, the hydroxyl profile is of the hydroxyl oxygen only; and the water profile is of the water oxygen atoms only.

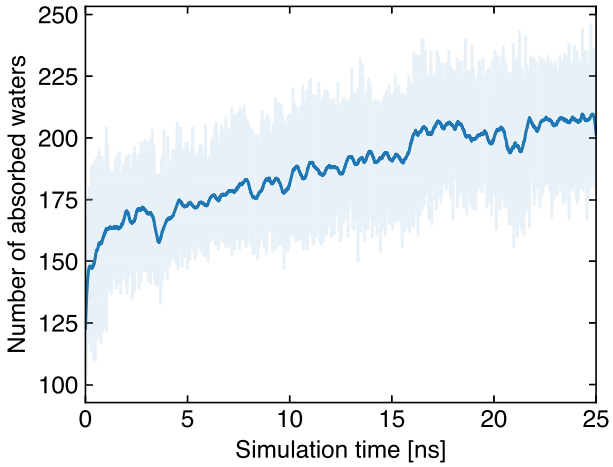

FIG. 5. Number of water absorbed into the CAS slab as a function of simulation time, where the light blue line indicates the raw calculated data, and the dark blue line shows the same data filtered.

structure at both the lower and upper interfaces exhibits a double peak or shoulder-to-peak-like profile. Coordination analysis of the calcium ions finds that no calcium ions completely detached from the CAS surface after 25 ns of water exposure.

Figures 4(c) and 4(d) show simplified number density profiles baselined to the hydroxyl oxygen peak at the lower and upper CAS-water interfaces, respectively. Here, all CAS network atoms excluding hydroxyl oxygen and hydrogen are summed and shown in green lines, hydroxyl oxygen is shown in orange, and the water oxygen is shown in blue. Density profiles taken at 1 ns are indicated with solid lines, and 24.5 ns profiles are indicated by dashed lines. Comparing dashed and solid lines, a very slight increase in water number density beyond the hydroxyl peak can be observed, i.e., more water has been absorbed past the defined CAS surface over the 25 ns of simulation.

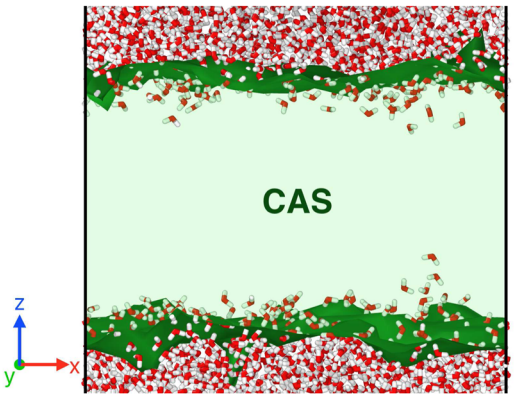

FIG. 6. The CAS-water interface after 25 ns of MD simulation with water shown in a molecular representation and the CAS slab represented in solid green, with the atomistic detail of the CAS not shown for clarity. Solid black lines indicate the periodic boundary of the simulation cell noting that some of this cell is not shown.

To quantify the amount of water absorbed by the CAS slab, the z coordinate of the hydroxyl oxygen density peak was used as a proxy measure for the location of the two CAS surfaces, thereby defining the volume of the CAS slab within the periodic cell. Figure 5 shows the number of water molecules that were located within the CAS volume at each ps, with raw data shown in light blue and filtered data indicated by the dark blue line. For the purposes of this calculation, the waters within the CAS volume can be considered absorbed within the CAS. The number of absorbed water molecules increases at a linear rate from ~2 to ~17 ns, after which the absorption rate decreases significantly, almost plateauing. Figure 6 shows an image of the CAS-water periodic cell from the last frame of the trajectory, i.e., at 25 ns, where the CAS slab is represented in green solid and the water is shown in the standard molecular representation. Only a relatively small amount of water has been absorbed past the CAS surface, with very few waters located deeper than ~5 Å below the surface.

Hydrogen bonding between water-CAS and CAS-CAS sites was stratified every picosecond to characterize the behavior of water at the interface. Figure 7 shows smoothed hydrogen bonding data for donating–accepting interactions as a function of simulation time on two different y-axis scales and ranges. Hydroxyl-water hydrogen bond counts remained consistent after the first nanosecond of simulation, indicating that the interface was saturated almost immediately and remained so throughout the simulation. However,

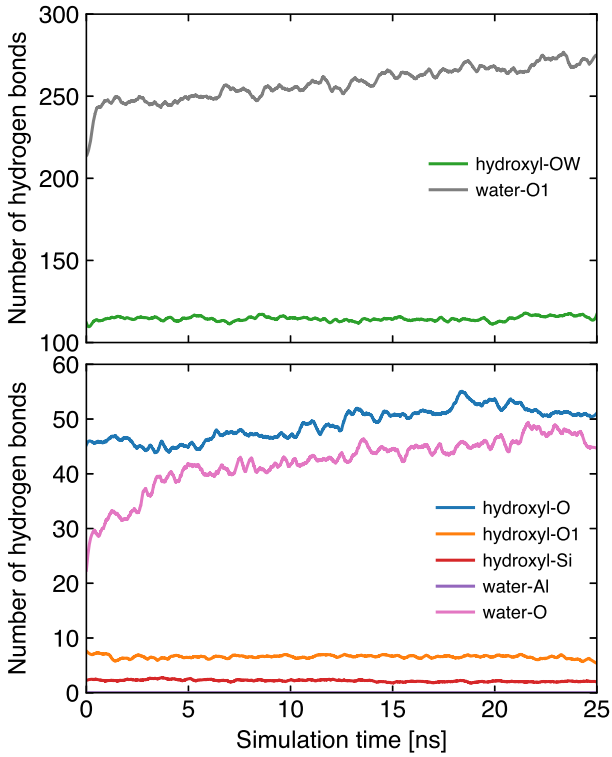

FIG. 7. Total number of hydrogen bonds (filtered) between the CAS slab and water as a function of simulation time, where the legend labels denote the donating group and acceptor site, respectively.

water–hydroxyl (water–O1) interaction counts increased from ~250 to 275 at a constant rate after the first nanosecond, suggesting the presence of water. This corresponds to the increase in water density behind the hydroxyl density peaks after 25 ns of simulation shown in Figs. 4(c) and 4(d). These data suggest that the interphase region may swell and spatially reorganize to accommodate additional water absorption throughout the simulation.

Considering intra-CAS interactions, hydrogen bonds between hydroxyl and network oxygen interactions increased a small amount, whereas hydroxyl–hydroxyl and hydroxyl–silicon remain constant. The number of hydrogen bonding interactions between water and network oxygen increased from 20 to 45 in a three stage manner: an initial rapid increase between 0 and 5 ns, a secondary slower increasing period between 5 and 20 ns, followed by a plateau. By assuming that the CAS interphase is fully saturated with water by around 5 ns, it is shown in Fig. 5 that ~30 or so water molecules were absorbed beyond the rough CAS surface and into either the interphase or bulk over the course of the simulation. The hydrogen bonding data, absorbed water count, and visual inspection confirmed that only 30 or fewer water molecules actually absorbed past the CAS surface, and even fewer progressed past the CAS interphase within 25 ns.

IV. CONCLUSION

A classical MD force-field capable of modeling calcium aluminosilicate (CAS) glass surfaces in contact with liquid water, termed wet-GS, was introduced by extending the GS FF to include the SPC/E water model. In addition, a surface preparation protocol was devised to capture the response of the CAS surface upon exposure to ambient moisture prior to immersion in liquid water. The cross-terms in the wet-GS force field were fitted to water structure data for several crystal oxide-water interfaces, including *ab initio* molecular dynamics simulations performed in this work for the wüstite and periclase aqueous interfaces. To showcase the wet-GS FF, MD simulations of a CAS slab that was interfaced with liquid water were performed. The simulations indicate that water saturates the CAS interface almost instantly and that a slower mode of water ingress throughout the CAS interphase takes over after 5 ns of dynamics. Water ingress into the bulk CAS network was limited to a few molecules over a course of 25 ns, suggesting the CAS water interface is relatively stable on the nanosecond timescale after incipient interphase saturation. The interatomic force field and CAS-water MD simulations introduced in this article provide the necessary platform for supporting further study of the free energy of dissolution of calcium from CAS glass and stone wool fiber, a critical aspect in elucidating dissolution of these materials.

SUPPLEMENTARY MATERIAL

The supplementary material contains additional detail about the simulation methodology and additional data to support the conclusions reported here.

ACKNOWLEDGMENTS

The authors gratefully acknowledge ROCKWOOL A/S for supporting this research. This research was undertaken with the assistance of resources from the National Computational Infrastructure (NCI Australia), an NCRIS-enabled capability supported by the Australian Government.

AUTHOR DECLARATIONS

Conflict of Interest

The authors have no conflicts to disclose.

Author Contributions

F. Vuković: Data curation (equal); Formal analysis (equal); Investigation (equal); Methodology (equal); Software (equal); Visualization (equal); Writing – original draft (equal); Writing – review & editing (equal). **N. A. Garcia**: Formal analysis (equal); Investigation (equal); Methodology (equal); Visualization (equal); Writing – review & editing (equal). **S. Perera**: Investigation (equal); Writing – original draft (equal). **M. Turchi**: Data curation (equal); Formal analysis (equal); Investigation (equal); Methodology (equal); Visualization (equal); Writing – review & editing (equal). **M. P. Andersson**: Resources (equal); Writing – review & editing (equal). **M. Solvang**: Funding acquisition (equal); Project administration (equal); Writing – review & editing (equal). **P. Raiteri**: Conceptualization (equal); Formal analysis (equal); Investigation (equal); Methodology (equal); Resources (equal); Supervision (equal); Writing – original draft (equal); Writing – review & editing (equal). **T. R. Walsh**: Conceptualization (equal); Funding acquisition (equal); Project administration (equal); Resources (equal); Supervision (equal); Writing – original draft (equal); Writing – review & editing (equal).

DATA AVAILABILITY

The data that support the findings of this study are available from the corresponding author upon reasonable request.

REFERENCES

[1] D. V. Okhrimenko, C. F. Nielsen, L. Z. Lakshtanov, K. N. Dalby, D. B. Johansson, M. Solvang, J. Deubener, and S. L. S. Stipp, "Surface reactivity and dissolution properties of alumina–silica glasses and fibers," ACS Appl. Mater. Interfaces **12**, 36740–36754 (2020).

[2] G. Gutiérrez and B. Johansson, "Molecular dynamics study of structural properties of amorphous Al_2O_3," Phys. Rev. B **65**, 104202 (2002).

[3] J. Horbach and W. Kob, "Static and dynamic properties of a viscous silica melt," Phys. Rev. B **60**, 3169–3181 (1999).

[4] A. Grossfield, P. Ren, and J. W. Ponder, "Ion solvation thermodynamics from simulation with a polarizable force field," J. Am. Chem. Soc. **125**, 15671–15682 (2003).

[5] P. Kollman, "Free energy calculations: Applications to chemical and biochemical phenomena," Chem. Rev. **93**, 2395–2417 (1993).

[6] A. C. T. van Duin, S. Dasgupta, F. Lorant, and W. A. Goddard, "ReaxFF: A reactive force field for hydrocarbons," J. Phys. Chem. A **105**, 9396–9409 (2001).

[7] L. Liu, A. Jaramillo-Botero, W. A. Goddard, and H. Sun, "Development of a ReaxFF reactive force field for ettringite and study of its mechanical failure modes from reactive dynamics simulations," J. Phys. Chem. A **116**, 3918–3925 (2012).

[8] A. C. T. van Duin, A. Strachan, S. Stewman, Q. Zhang, X. Xu, and W. A. Goddard, "$ReaxFF_{SiO}$ reactive force field for silicon and silicon oxide systems," J. Phys. Chem. A **107**, 3803–3811 (2003).

[9]H. Manzano, R. J. M. Pellenq, F.-J. Ulm, M. J. Buehler, and A. C. T. van Duin, "Hydration of calcium oxide surface predicted by reactive force field molecular dynamics," Langmuir **28**, 4187–4197 (2012).
[10]A. D. Kulkarni, D. G. Truhlar, S. Goverapet Srinivasan, A. C. T. van Duin, P. Norman, and T. E. Schwartzentruber, "Oxygen interactions with silica surfaces: Coupled cluster and density functional investigation and the development of a new ReaxFF potential," J. Phys. Chem. C **117**, 258–269 (2012).
[11]M. C. Pitman and A. C. T. van Duin, "Dynamics of confined reactive water in smectite clay–zeolite composites," J. Am. Chem. Soc. **134**, 3042–3053 (2012).
[12]S. H. Hahn and A. C. T. van Duin, "Surface reactivity and leaching of a sodium silicate glass under an aqueous environment: A ReaxFF molecular dynamics study," J. Phys. Chem. C **123**, 15606–15617 (2019).
[13]J. Yang, D. Hou, and Q. Ding, "Structure, dynamics, and mechanical properties of cross-linked calcium aluminosilicate hydrate: A molecular dynamics study," ACS Sustainable Chem. Eng. **6**, 9403–9417 (2018).
[14]R. T. Cygan, J. J. Liang, and A. G. Kalinichev, "Molecular models of hydroxide, oxyhydroxide, and clay phases and the development of a general force field," J. Phys. Chem. B **108**, 1255–1266 (2004).
[15]B. Guillot and N. Sator, "A computer simulation study of natural silicate melts. Part I: Low pressure properties," Geochim. Cosmochim. Acta **71**, 1249–1265 (2007).
[16]M. Turchi, S. Perera, S. Ramsheh, A. J. Popel, D. V. Okhrimenko, S. L. S. Stipp, M. Solvang, M. P. Andersson, and T. R. Walsh, "Predicted structures of calcium aluminosilicate glass as a model for stone wool fiber: Effects of composition and interatomic potential," J. Non-Cryst. Solids **567**, 120924 (2021).
[17]S. Sundararaman, L. Huang, S. Ispas, and W. Kob, "New interaction potentials for alkali and alkaline-earth aluminosilicate glasses," J. Chem. Phys. **150**, 154505 (2019).
[18]A. A. Freitas, R. L. Santos, R. Colaço, R. Bayão Horta, and J. N. Canongia Lopes, "From lime to silica and alumina: Systematic modeling of cement clinkers using a general force-field," Phys. Chem. Chem. Phys. **17**, 18477–18494 (2015).
[19]B. P. Feuston and S. H. Garofalini, "Water-induced relaxation of the vitreous silica surface," J. Appl. Phys. **68**, 4830–4836 (1990).
[20]B. P. Feuston and S. H. Garofalini, "Oligomerization in silica sols," J. Phys. Chem. **94**, 5351–5356 (1990).
[21]F. H. Stillinger and A. Rahman, "Revised central force potentials for water," J. Chem. Phys. **68**, 666–670 (1978).
[22]E. R. Cruz-Chu, A. Aksimentiev, and K. Schulten, "Water–silica force field for simulating nanodevices," J. Phys. Chem. B **110**, 21497–21508 (2006).
[23]T. S. Mahadevan and S. H. Garofalini, "Dissociative chemisorption of water onto silica surfaces and formation of hydronium ions," J. Phys. Chem. C **112**, 1507–1515 (2008).
[24]D. A. Litton and S. H. Garofalini, "Modeling of hydrophilic wafer bonding by molecular dynamics simulations," J. Appl. Phys. **89**, 6013–6023 (2001).
[25]B. P. Feuston and S. H. Garofalini, "Empirical three-body potential for vitreous silica," J. Chem. Phys. **89**, 5818–5824 (1988).
[26]A. A. Hassanali and S. J. Singer, "Model for the water–amorphous silica interface: The undissociated surface," J. Phys. Chem. B **111**, 11181–11193 (2007).
[27]H. J. C. Berendsen, J. R. Grigera, and T. P. Straatsma, "The missing term in effective pair potentials," J. Phys. Chem. **91**, 6269–6271 (1987).
[28]B. W. H. van Beest, G. J. Kramer, and R. A. van Santen, "Force fields for silicas and aluminophosphates based on *ab initio* calculations," Phys. Rev. Lett. **64**, 1955–1958 (1990).
[29]A. Butenuth, G. Moras, J. Schneider, M. Koleini, S. Köppen, R. Meißner, L. B. Wright, T. R. Walsh, and L. C. Ciacchi, "*Ab initio* derived force-field parameters for molecular dynamics simulations of deprotonated amorphous-SiO_2/water interfaces," Phys. Status Solidi B **249**, 292–305 (2011).
[30]S. Leroch and M. Wendland, "Simulation of forces between humid amorphous silica surfaces: A comparison of empirical atomistic force fields," J. Phys. Chem. C **116**, 26247–26261 (2012).
[31]T. S. Mahadevan and J. Du, "Evaluating water reactivity at silica surfaces using reactive potentials," J. Phys. Chem. C **122**, 9875–9885 (2018).
[32]J. M. Rimsza and J. Du, "Interfacial structure and evolution of the water–silica gel system by reactive force-field-based molecular dynamics simulations," J. Phys. Chem. C **121**, 11534–11543 (2017).
[33]T. Du, H. Li, G. Sant, and M. Bauchy, "New insights into the sol–gel condensation of silica by reactive molecular dynamics simulations," J. Chem. Phys. **148**, 234504 (2018).
[34]L. Deng, K. Miyatani, S. I. Amma, M. Suehara, M. Ono, Y. Yamamoto, S. Urata, and J. Du, "Reaction mechanisms and interfacial behaviors of sodium silicate glass in an aqueous environment from reactive force field-based molecular dynamics simulations," J. Phys. Chem. C **123**, 21538–21547 (2019).
[35]J. Kalahe, T. S. Mahadevan, M. Ono, K. Miyatani, S. Urata, and J. Du, "Composition effect on interfacial reactions of sodium aluminosilicate glasses in aqueous solution," J. Phys. Chem. B **127**, 269–284 (2023).
[36]P. Ugliengo, V. Saunders, and E. Garrone, "Silanol as a model for the free hydroxyl of amorphous silica: Ab-initio calculations of the interaction with water," J. Phys. Chem. **94**, 2260–2267 (1990).
[37]A. Rimola and P. Ugliengo, "A quantum mechanical study of the reactivity of $(SiO)_2$-defective silica surfaces," J. Chem. Phys. **128**, 204702 (2008).
[38]F. Musso, P. Mignon, P. Ugliengo, and M. Sodupe, "Cooperative effects at water–crystalline silica interfaces strengthen surface silanol hydrogen bonding. An *ab-initio* molecular dynamics study," Phys. Chem. Chem. Phys. **14**, 10507 (2012).
[39]M. Sulpizi, M.-P. Gaigeot, and M. Sprik, "The silica–water interface: How the silanols determine the surface acidity and modulate the water properties," J. Chem. Theory Comput. **8**, 1037–1047 (2012).
[40]K. Yuan, N. Rampal, P. Fenter, J. D. Kubicki, A. G. Stack, and S. Irle, "Density functional tight-binding simulations reveal the presence of surface defects on the quartz (101)–water interface," J. Phys. Chem. C **125**, 16246–16255 (2021).
[41]T. Mahadevan, A. Baroni, M. Taron, S. Gin, J. Du, and J.-M. Delaye, "Development of potentials for molecular dynamics simulations of dry and hydrated calcium aluminosilicate glasses by force matching and refinement," J. Non-Cryst. Solids **592**, 121746 (2022).
[42]R. Wang, M. L. Klein, V. Carnevale, and E. Borguet, "Investigations of water/oxide interfaces by molecular dynamics simulations," Wiley Interdiscip. Rev.: Comput. Mol. Sci. **11**, e1537 (2021).
[43]K. J. Harmon, K. Letchworth-Weaver, A. P. Gaiduk, F. Giberti, F. Gygi, M. K. Y. Chan, P. Fenter, and G. Galli, "Validating first-principles molecular dynamics calculations of oxide/water interfaces with x-ray reflectivity data," Phys. Rev. Mater. **4**, 113805 (2020).
[44]A. P. Thompson, H. M. Aktulga, R. Berger, D. S. Bolintineanu, W. M. Brown, P. S. Crozier, P. J. in't Veld, A. Kohlmeyer, S. G. Moore, T. D. Nguyen, R. Shan, M. J. Stevens, J. Tranchida, C. Trott, and S. J. Plimpton, "LAMMPS—A flexible simulation tool for particle-based materials modeling at the atomic, meso, and continuum scales," Comput. Phys. Commun. **271**, 108171 (2022).
[45]R. Hockney and J. Eastwood, *Computer Simulation Using Particles* (CRC Press, 1988).
[46]G. J. Martyna, D. J. Tobias, and M. L. Klein, "Constant pressure molecular dynamics algorithms," J. Chem. Phys. **101**, 4177–4189 (1994).
[47]A. Stukowski, "Visualization and analysis of atomistic simulation data with OVITO—The Open Visualization Tool," Modell. Simul. Mater. Sci. Eng. **18**, 015012 (2009).
[48]T. D. Kühne, M. Iannuzzi, M. D. Ben, V. V. Rybkin, P. Seewald, F. Stein, T. Laino, R. Z. Khaliullin, O. Schütt, F. Schiffmann, D. Golze, J. Wilhelm, S. Chulkov, M. H. Bani-Hashemian, V. Weber, U. Borštnik, M. Taillefumier, A. S. Jakobovits, A. Lazzaro, H. Pabst, T. Müller, R. Schade, M. Guidon, S. Andermatt, N. Holmberg, G. K. Schenter, A. Hehn, A. Bussy, F. Belleflamme, G. Tabacchi, A. Glöß, M. Lass, I. Bethune, C. J. Mundy, C. Plessl, M. Watkins, J. VandeVondele, M. Krack, and J. Hutter, "CP2K: An electronic structure and molecular dynamics software package—Quickstep: Efficient and accurate electronic structure calculations," J. Chem. Phys. **152**, 194103 (2020).
[49]J. P. Perdew, K. Burke, and M. Ernzerhof, "Generalized gradient approximation made simple," Phys. Rev. Lett. **77**, 3865–3868 (1996).
[50]M. Alfredsson, G. David Price, C. R. A. Catlow, S. C. Parker, R. Orlando, and J. P. Brodholt, "Electronic structure of the antiferromagnetic *B*1 structured FeO," Phys. Rev. B **70**, 165111 (2004).
[51]V. I. Anisimov, J. Zaanen, and O. K. Andersen, "Band theory and Mott insulators: Hubbard *U* instead of Stoner *I*," Phys. Rev. B **44**, 943–954 (1991).
[52]P. Liao and E. A. Carter, "*Ab initio* DFT + *U* predictions of tensile properties of iron oxides," J. Mater. Chem. **20**, 6703–6719 (2010).

[53]S. L. Dudarev, G. A. Botton, S. Y. Savrasov, C. J. Humphreys, and A. P. Sutton, "Electron-energy-loss spectra and the structural stability of nickel oxide: An LSDA+U study," Phys. Rev. B **57**, 1505–1509 (1998).
[54]G. Bussi, D. Donadio, and M. Parrinello, "Canonical sampling through velocity rescaling," J. Chem. Phys. **126**, 014101 (2007).
[55]E. Schwegler, J. C. Grossman, F. Gygi, and G. Galli, "Towards an assessment of the accuracy of density functional theory for first principles simulations of water. II," J. Chem. Phys. **121**, 5400–5409 (2004).
[56]B. Armstrong, A. Silvestri, R. Demichelis, P. Raiteri, and J. D. Gale, "Solubility-consistent force field simulations for aqueous metal carbonate systems using graphical processing units," Philos. Trans. R. Soc., A **381**, 20220250 (2023).
[57]L. Martínez, R. Andrade, E. G. Birgin, and J. M. Martínez, "PACKMOL: A package for building initial configurations for molecular dynamics simulations," J. Comput. Chem. **30**, 2157–2164 (2009).
[58]M. Lingenheil, R. Denschlag, R. Reichold, and P. Tavan, "The 'hot-solvent/cold-solute' problem revisited," J. Chem. Theory Comput. **4**, 1293–1306 (2008).
[59]P. H. Hünenberger, "Thermostat algorithms for molecular dynamics simulations," in *Advanced Computer Simulation* (Springer, Berlin, Heidelberg, 2005), pp. 105–149.
[60]N. Michaud-Agrawal, E. J. Denning, T. B. Woolf, and O. Beckstein, "MDAnalysis: A toolkit for the analysis of molecular dynamics simulations," J. Comput. Chem. **32**, 2319–2327 (2011).
[61]R. Gowers, M. Linke, J. Barnoud, T. Reddy, M. Melo, S. Seyler, J. Domański, D. Dotson, S. Buchoux, I. Kenney, and O. Beckstein, "MDAnalysis: A Python package for the rapid analysis of molecular dynamics simulations," in Proceedings of the Python in Science Conference (SciPy, 2016), 2016.
[62]P. Smith, R. M. Ziolek, E. Gazzarrini, D. M. Owen, and C. D. Lorenz, "On the interaction of hyaluronic acid with synovial fluid lipid membranes," Phys. Chem. Chem. Phys. **21**, 9845–9857 (2019).
[63]A. Savitzky and M. J. E. Golay, "Smoothing and differentiation of data by simplified least squares procedures," Anal. Chem. **36**, 1627–1639 (1964).
[64]N. H. de Leeuw, J. A. Purton, S. C. Parker, G. W. Watson, and G. Kresse, "Density functional theory calculations of adsorption of water at calcium oxide and calcium fluoride surfaces," Surf. Sci. **452**, 9–19 (2000).
[65]H. S. Craft, R. Collazo, M. D. Losego, Z. Sitar, and J.-P. Maria, "Surface water reactivity of polycrystalline MgO and CaO films investigated using x-ray photoelectron spectroscopy," J. Vac. Sci. Technol. A **26**, 1507–1510 (2008).
[66]K. Johannsen and S. Rademacher, "Modelling the kinetics of calcium hydroxide dissolution in water," Acta Hydrochim. Hydrobiol. **27**, 72–78 (1999).
[67]P. López-Arce, L. S. Gómez-Villalba, S. Martínez-Ramírez, M. Álvarez de Buergo, and R. Fort, "Influence of relative humidity on the carbonation of calcium hydroxide nanoparticles and the formation of calcium carbonate polymorphs," Powder Technol. **205**, 263–269 (2011).
[68]M. K. Ridley and D. Tunega, "Insights on the structural and dynamic properties of corundum–water interfaces from first-principle molecular dynamics," J. Phys. Chem. C **125**, 295–309 (2020).
[69]J. G. Catalano, "Weak interfacial water ordering on isostructural hematite and corundum (001) surfaces," Geochim. Cosmochim. Acta **75**, 2062–2071 (2011).
[70]J. Janeček, R. R. Netz, M. Flörsheimer, R. Klenze, B. Schimmelpfennig, and R. Polly, "Influence of hydrogen bonding on the structure of the (001) corundum–water interface. Density functional theory calculations and Monte Carlo simulations," Langmuir **30**, 2722–2728 (2014).
[71]F. Bellucci, S. S. Lee, J. D. Kubicki, A. Bandura, Z. Zhang, D. J. Wesolowski, and P. Fenter, "Rb^+ adsorption at the quartz(101)–aqueous interface: Comparison of resonant anomalous X-ray reflectivity with ab initio calculations," J. Phys. Chem. C **119**, 4778–4788 (2015).
[72]J. Rey, S. Blanck, P. Clabaut, S. Loehlé, S. N. Steinmann, and C. Michel, "Transferable Gaussian attractive potentials for organic/oxide interfaces," J. Phys. Chem. B **125**, 10843–10853 (2021).
[73]K. Jug, B. Heidberg, and T. Bredow, "Cyclic cluster study of water adsorption structures on the MgO(100) surface," Surf. Sci. **601**, 1529–1535 (2007).
[74]W. Loewenstein, "The distribution of aluminum in the tetrahedra of silicates and aluminates," Am. Mineral. **39**, 92–96 (1954).
[75]J. F. Stebbins, E. V. Dubinsky, K. Kanehashi, and K. E. Kelsey, "Temperature effects on non-bridging oxygen and aluminum coordination number in calcium aluminosilicate glasses and melts," Geochim. Cosmochim. Acta **72**, 910–925 (2008).
[76]S. K. Lee and J. F. Stebbins, "Al–O–Al and Si–O–Si sites in framework aluminosilicate glasses with Si/Al = 1: Quantification of framework disorder," J. Non-Cryst. Solids **270**, 260–264 (2000).
[77]S. K. Lee and J. F. Stebbins, "The structure of aluminosilicate glasses: High-resolution ^{17}O and ^{27}Al MAS and 3QMAS NMR study," J. Phys. Chem. B **104**, 4091–4100 (2000).